chemosensors

MDPI

Article

The Functional Fe_3O_4@SiO_2@AuNPs SERS Nanomaterials for Rapid Enrichment and Detection of Mercury Ions in Licorice

Jieqiang Zhu [1], Baoling Wang [1], Ping Yang [1], Junmei Li [1], Guyu Xiao [1], Jiangyu Yao [1], Xingchu Gong [2], Jizhong Yan [1] and Hui Zhang [1,*]

[1] College of Pharmaceutical Science, Zhejiang University of Technology, No. 18 Chaowang Road, Hangzhou 310014, China
[2] Pharmaceutical Informatics Institute, College of Pharmaceutical Sciences, Zhejiang University, Hangzhou 310058, China
* Correspondence: zh889@zjut.edu.cn; Tel.: +86-0571-8832-0984; Fax: +86-0571-8832-0984

Abstract: There has been an increasing demand for rapid and sensitive techniques for the detection of heavy metal ions that are harmful to the human body in traditional Chinese medicine (TCM). However, the complex chemical composition of TCM makes the quantitative detection of heavy metal ions difficult. In this study, the magnetic Fe_3O_4@SiO_2@AuNPs nanoparticles combined with a probe molecule DMcT were used for the specific enrichment and detection of Hg^{2+} in the complex system of licorice. The core of Fe_3O_4 was bonded with SiO_2 to increase its stability. A layer of AuNPs was deposited to produce a "core–shell" Raman substrate with high surface-enhanced Raman spectroscopy (SERS) activity, which was surface modified by DMcT probe molecules with sulfhydryl groups. In the presence of Hg^{2+}, Hg^{2+} binds to N on the amino group of DMcT to form N-Hg^{2+}-N complexes, which induces Fe_3O_4@SiO_2@AuNPs-DMcT clustering to enhance SERS signal. The Raman probe molecule DMcT showed an excellent linear relationship (R^2 = 0.9709) between the SERS signal at 1416 cm^{-1} and the Hg^{2+} concentration (0.5~100 ng/mL). This method achieved a good recovery (89.10~111.00%) for the practical application of detection of Hg^{2+} in licorice extracts. The results demonstrated that the functional Fe_3O_4@SiO_2@AuNPs-DMcT performed effective enrichment and showed high sensitivity and accurate detection of heavy metal ions from the analytes.

Keywords: surface-enhanced Raman spectroscopy; magnetic nanoparticles; mercury ions; traditional Chinese medicine; licorice extracts; Fe_3O_4@SiO_2@AuNPs

check for updates

Citation: Zhu, J.; Wang, B.; Yang, P.; Li, J.; Xiao, G.; Yao, J.; Gong, X.; Yan, J.; Zhang, H. The Functional Fe_3O_4@SiO_2@AuNPs SERS Nanomaterials for Rapid Enrichment and Detection of Mercury Ions in Licorice. *Chemosensors* **2022**, *10*, 403. https://doi.org/10.3390/chemosensors10100403

Academic Editor: Barbara Palys

Received: 31 August 2022
Accepted: 4 October 2022
Published: 8 October 2022

1. Introduction

Traditional Chinese medicine (TCM), which uses medicinal substances derived mainly from plants, minerals, and animal substances, has been used worldwide to treat various diseases, especially during COVID-19 [1,2]. Licorice is one of the most popular TCM, called Gan-Cao in China. It is derived from the dried roots and rhizomes of *Glycyrrhiza uralensis*, *G. glabra*, and *G. inflata*, and is recorded in the pharmacopoeias of China, Japan, US, and Europe.

Due to the increasing demand for TCM worldwide, their safety has become a hot topic of international concern [3]. Most of the hazards associated with TCM come from contamination by toxic heavy metal ions, including lead (Pb^{2+}), arsenic (As^{3+}), cadmium (Cd^{2+}), and mercury (Hg^{2+}) [4]. In particular, mercury ions (Hg^{2+}), as the most toxic liquid heavy metal ions, are bioaccumulative and highly enriched, posing a severe threat to humans and the environment even at low concentrations [5–7]. It is estimated that poisoning and neurological symptoms may occur once an adult has 50 μg/g of Hg^{2+} in hair or 0.4 μg/g of Hg^{2+} in red blood cells. Currently, Hg^{2+} poisoning has become one of the most severe contamination problems in TCM.

The traditional techniques for detection of heavy metals include inductively coupled plasma mass spectrometry (ICP-MS) [8], atomic absorption spectrometry (AAS) [9], electrochemical methods [10], fluorescence methods [11], inductively coupled plasma emission spectrometry (ICP-OES) [12], and colorimetric methods [13]. Most of these are stable and accurate, yet bulky instruments and toxic reagents restrict the application in routine analysis. There are generally problems with these techniques, such as cumbersome pre-treatment, long detection cycles, and expensive detection costs. Therefore, it is of great practical importance to construct a simple, rapid, and accurate technique for the detection of heavy metal ions.

Surface-enhanced Raman spectroscopy (SERS) is a fingerprint spectroscopy method with ultra-high sensitivity [14–16]. SERS contains a large amount of information about the properties of substances. It provides not only highly sensitive fingerprint spectral characteristics of molecules, but also has many other advantages, such as simple operation, strong anti-interference ability, high selectivity, rapid non-destructive detection, and equipment miniaturization. Currently, it is widely used in food safety, biomedicine, environmental testing, and defense protection [17–19]. However, heavy metal ions are a class of inorganic substances that usually exist in the environment in a monoatomic state, which cannot be detected directly using SERS because of their small scattering cross-section [20]. Currently, SERS detection of Hg^{2+} consists of the SERS signal "turn-on" mode and "turn-down" mode [21]. Since SERS has been used to detect Hg^{2+}, the preparation of SERS substrates has gradually become a hot research topic.

However, the current conventional single precious metal Raman-active substrates, such as AgNPs and AuNPs, are soluble and prone to agglomeration, poor stability, and low sensitivity. To solve these issues, researchers have proposed various methods to construct SERS substrates with high sensitivity, stability, and selectivity. Wang et al. [22] prepared high-performance Fe_3O_4@SiO_2@Ag using the seed-mediated method and verified the performance of the substrate using 4-Aminothiophenol and thiram, with detection limits of 10^{-11} mol/L and 10^{-9} mol/L, respectively. Xu et al. [23] prepared Fe_3O_4@SiO_2@Ag magnetic material using the crystal seed method and achieved the separation and enrichment of benzocillin under the action of an applied magnetic field with a detection limit of 10^{-11} mol/L. Wang et al. [24] reported Fe_3O_4@PEG@Ag nanoliters were synthesized and performed well in cell imaging and cancer quality detection. Shen et al. [25] reported novel multifunctional Fe_3O_4@Ag/SiO_2/Au core–shell microspheres with a unique nanostructure using rhodamine-b (RdB) as a probe molecule in Raman activity studies. Sun et al. [26] designed a versatile core–satellite Fe_3O_4@SiO_2-Au (FA) hetero-nanostructure and demonstrated its use for active adsorption and selective detection of food dye molecules. In Alexey et al. [27], Cisplatin (cPt) was successfully immobilized on the surface of Fe_3O_4@SiO_2@Au nanoparticles (NPs). The functionalized Fe_3O_4@SiO_2@AuNPs were tested for potential application in photothermal cancer therapy.

The literature review showed that there are few reports on the application of magnetic nanomaterials combined with SERS in the detection of mercury ions in TCM. However, the 2020 version of the Chinese pharmacopoeia has put forward higher requirements for the inspection of heavy metal ions in different kinds of TCM, such as licorice. Therefore, it is necessary to develop a fast and on-site trace detection method for heavy metal ions to improve the quality of traditional Chinese medicines.

2. Materials and Methods

2.1. Materials and Apparatus

Mercury ion, lead ion, cadmium ion, arsenic ion, and copper ion standard solution (No: GBW 1000 μg/mL) were purchased from Zhongke Quality Inspection Biotechnology Co., Ltd. (Beijing, China). Triiron tetroxide (99%) was provided by Enochai Technology (Beijing, China). 48–50% $HAuCl_4$, 2,5-dimercapto-1,3,4-thiadiazole (97%, DMcT), 98% TEOS, and 98% APTES were purchased from Maclean (Shanghai, China). Anhydrous ethanol (99.7%, Yongda Chemical Reagent, Tianjin, China), 25~28% $NH_3 \cdot H_2O$, and 36–38%

hydrochloric acid were purchased from Sinopharm Chemical Reagent Co., Ltd. (Shanghai, China). N-butylamine (99%, Titan Technology Co., Ltd., Shanghai, China), nitric acid (99%, Yonghua Chemical Technology Co. Ltd., Jiangsu, China), and other reagents were all analytical grade.

Apparatuses used in the research included: a Scanning Electron Microscope (Hitachi, Japan), a UV-2450 ultraviolet spectrophotometer (Shimadzu, Japan), a XMTD-8222 vacuum drying oven (Jinghong Experiment, Shanghai, China), an intelligent double-controlled constant temperature magnetic stirrer (DF 101S, Hangzhou, China), a constant temperature digital display water bath (HH-4, Shanghai, China), a ProTT-EZRaman-B portable Raman spectrometer (Enwave Optronics, Irvine, CA, USA), an electronic balance (SQP, Sartorius Scientific Instruments, Beijing, China), an ultrasonic cleaner (KQ-250DB, Jiangsu, China), and a Milli-Q ultrapure water machine (Thermo Fisher Scientific, Shanghai, China).

2.2. Synthesis of Fe_3O_4@SiO_2

The synthesis of Fe_2O_3@SiO_2 was implemented using a modified Stöber method [28]. Briefly, 0.5 g Fe_3O_4 solid nanoparticles were dispersed in HCl (0.01 mol/L 20 mL) and ultrasonically dispersed for 10 min for activation and modification. Next, a magnet was used to separate the Fe_3O_4 from HCl and washed several times with ultrapure water to achieve neutrality. The modified Fe_3O_4 was then redispersed in a solution consisting of 80 mL ethanol and 20 mL water and sonicated for 45 min to make the Fe_3O_4 nanoparticles uniformly dispersed. A total of 4 mL of $NH_3 \cdot H_2O$ was added to the system (300–400 r/min) after complete dispersion, followed by 4 mL of TEOS (100 μL/min) slowly added drop by drop while stirring. The Fe_3O_4@SiO_2 nanoparticles were obtained by continuing stirring at room temperature for 6 h under N_2 protection. With the help of magnetic separation, the products were washed several times using anhydrous ethanol and ultrapure water, and dried under vacuum at 60 °C for 5 h.

2.3. Amination of Fe_3O_4@SiO_2

A total of 0.5 g of Fe_3O_4@SiO_2 prepared as described above was placed in a three-neck flask containing 40 mL of anhydrous ethanol, sonicated for 30 min, and then transferred to a constant-temperature water bath. Five milliliters of APTES (100 μL/min) was slowly added under mechanical stirring. The amination was carried out by stirring and refluxing at 80 °C for 6 h under the protection of N_2. After the reaction was completed, the nanoparticles were washed three times with anhydrous ethanol using ultrasonication with the help of an applied magnetic field. Finally, the aminated Fe_3O_4@SiO_2 was isolated and then dried under vacuum at 60–70 °C for 6 h.

2.4. Synthesis of Fe_3O_4@SiO_2@AuNPs

For the preparation of AuNPs, 5 mg of $HAuCl_4$-H_2O was dissolved in 60 mL of ultrapure water and heated to boiling at 120 °C in a water bath at reflux. The reaction lasted for 6 min to see the change of the solution color from colorless to burgundy. AuNPs were then obtained and cooled at room temperature.

Six milligrams of the aminated Fe_3O_4@SiO_2 was dispersed in 10 mL of ultrapure water and sonicated for 10 min to dissolve it thoroughly. A total of 40 mL of the prepared AuNPs was then added and stirred for 40 min. The prepared Fe_3O_4@SiO_2@AuNPs were magnetically separated with an applied magnetic force and washed several times using anhydrous ethanol and ultrapure water. Finally, they were dispersed in 10 mL of ultrapure water and stored at 4 °C for use.

2.5. Preparation of DMcT-Functionalized Fe_3O_4@SiO_2@AuNPs

An amount of 0.5 g Fe_3O_4@SiO_2@AuNPs was uniformly dispersed in 10 mL of ultrapure water with 5 mL of DMcT (10^{-4} mol/L) and incubated by shaking for 1 h on a digital shaker (25 °C, 140 r/min). The DMcT-functionalized Fe_3O_4@SiO_2@AuNPs were finally dispersed in 10 mL of ultrapure water and stored at 4 °C for use.

2.6. Sample Preparation and Raman Spectroscopy Analytical Parameters

For the preparation of standard Hg^{2+} solution, the Hg^{2+} standard solution (1000 μg/mL) was diluted to different concentrations (0.1~100 ng/mL) with ultrapure water. A total of 200 μL Fe_3O_4@SiO_2@AuNPs-DMcT was mixed thoroughly with equal amounts of target samples at room temperature for SERS detection.

To process the licorice samples, licorice herbs were powdered and sieved, and 5 g of powder was added to 50 mL of water for 30 min of sonication, then centrifuged and passed through a 0.22 μm filter membrane to remove insoluble impurities. Next, a series of Hg^{2+} standard solutions were added, and the sample was tested using SERS.

A portable Raman spectrometer with a laser wavelength of 785 nm and an excitation power of 350 mW was used. The acquisition time for each spectrum was set to 10 s and accumulated three times. The integration time and laser power were the same for all SERS samples unless otherwise stated.

2.7. Data Processing

The SERS spectra were plotted using Origin2019b 64Bit.lnk by comparing the data from five experiments to obtain the mean values. Background correction was performed for all spectra using the selective nonlinear iterative shear (SNIP) algorithm.

3. Results and Discussion

3.1. Synthesis and Characterization of Fe_3O_4@SiO_2@AuNPs

The Fe_3O_4@SiO_2@AuNPs were synthesized through layer-by-layer assembly. The preparation process of Fe_3O_4@SiO_2@AuNPs is shown in Scheme 1. First, the surface of Fe_3O_4 was covered with a SiO_2 protective shell to increase its stability and dispersibility, and then Fe_3O_4@SiO_2 was aminated and connected with AuNPs. The synthesized Fe_3O_4@SiO_2@AuNPs possessed the magnetic properties of Fe_3O_4 and the Raman-enhanced properties of AuNPs.

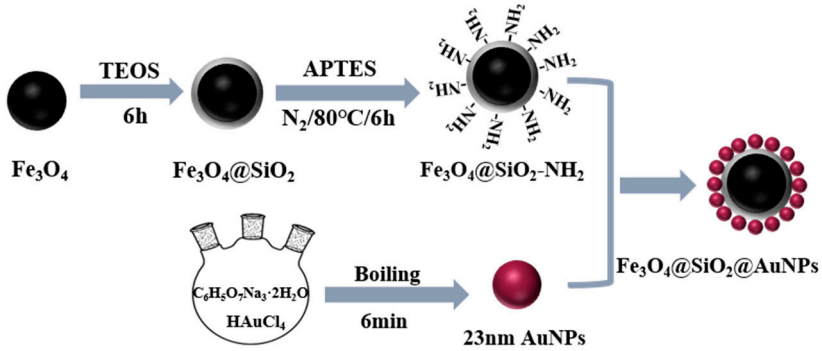

Scheme 1. Schematic diagram illustrating the synthesis of Fe_3O_4@SiO_2@AuNPs.

The prepared Fe_3O_4@SiO_2 was analyzed by scanning electron microscopy (SEM), and the results are shown in Figure 1A. The SEM image showed that the uncoated Fe_3O_4 particles were irregular in shape, with particle size around 30 nm and severe agglomeration between particles (Figure 1A(a)). To enhance the stability of the exposed Fe_3O_4 nanoparticles, SiO_2 was used to protect them. Figure 1A(b) showed the shape of Fe_3O_4@SiO_2 after coating, and it was apparent that the surface of Fe_3O_4 was covered with a gray SiO_2 nanolayer. The particle size was slightly regular with the average particle size around 50 nm. SEM images revealed that AuNPs randomly clustered around Fe_3O_4@SiO_2, and dense AuNPs wrapped the surface of Fe_3O_4@SiO_2. As shown in Figure 1B, the black dashed line indicates Fe_3O_4@SiO_2, which performed no significant UV absorption. The blue line indicates the UV absorption spectrum of Fe_3O_4@SiO_2@AuNPs, and the UV absorption peak at 520 nm shows the successful modification of AuNPs on the surface of Fe_3O_4@SiO_2. The red dashed line indicates the UV absorption spectrum of Fe_3O_4@SiO_2@AuNPs after the addition of Hg^{2+}. The SPR absorbance decreased after the addition of Hg^{2+} to the AuNP

solution and further red-shifted to 720 nm by the redox reaction between Hg^{2+} and AUNPs, leading to the formation of small AuNPs [29].

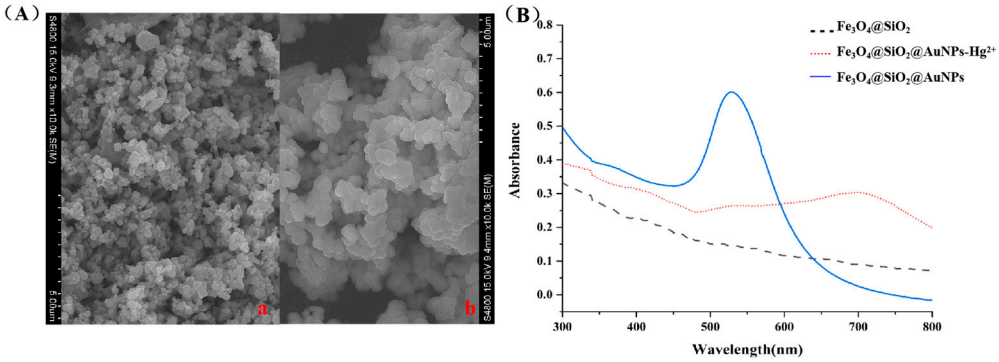

Figure 1. Characterization of Fe_3O_4@SiO_2. (**A**) Scanning electron microscopy (SEM), the shape of uncoated Fe_3O_4 particles (**a**), the shape of Fe_3O_4@SiO_2 after coating (**b**); (**B**) ultraviolet–visible spectroscopy (UV-Vis).

3.2. Magnetic Adsorption Performance of Fe_3O_4@SiO_2@AuNPs

To confirm the ability of magnetic adsorption of Hg^{2+} by Fe_3O_4@SiO_2, part of the dried powder was taken and ultrasonically dispersed near the magnetic frame. It could be seen that the solid powder was magnetically adsorbed quickly. Figure 2A shows the synthesis of Fe_3O_4@SiO_2. The remaining liquid was milky white after magnetic separation and clarified after several washes. Figure 2B shows that the aminated Fe_3O_4@SiO_2 retained prominent magnetic properties.

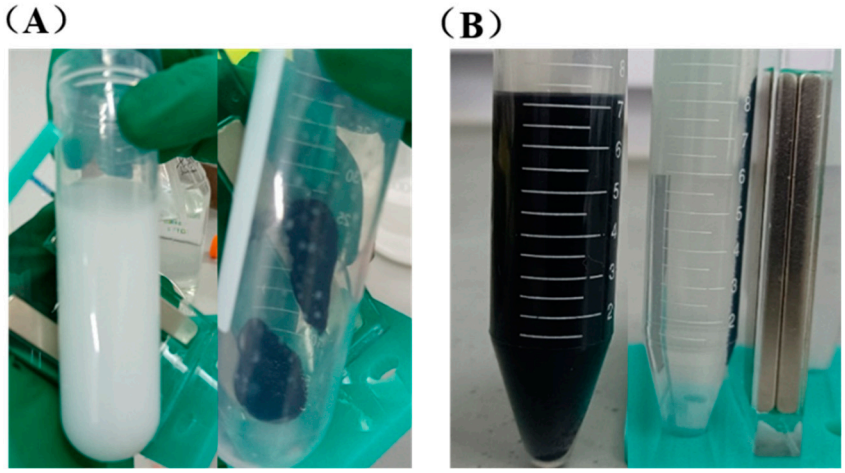

Figure 2. Photographs of magnetic nanomaterials before and after magnetic separation. (**A**) the mixing state (left) and the magnetic suction state (right) of Fe_3O_4@SiO_2; (**B**) the mixing state (left) and the magnetic suction state (right) of Aminated Fe_3O_4@SiO_2.

3.3. Principle of Hg^{2+} Detection Based on Fe_3O_4@SiO_2@AuNPs-DMcT

DMcT ($C_2H_2N_2S_3$) has four main donor sites, two -NH and two -SH. Its structural formula is shown in Figure 3. Previous experiments found that the two -SH groups on DMcT combined with Fe_3O_4@SiO_2@AuNPs. When Hg^{2+} was present in the system, the strong coordination binding between Hg^{2+} and the nitrogen atom in DMcT drove the aggregation of the Fe_3O_4@SiO_2@AuNPs-DMcT-Hg^{2+} sandwich structure, which significantly enhanced the SERS signal of DMcT. The Hg^{2+} detection solution was achieved by linking the amount of Hg^{2+} with the "hot spot" effect of NPs, and indirect detection of Hg^{2+} in samples was achieved by enhancement of Raman information. The detection principle is shown in Figure 3.

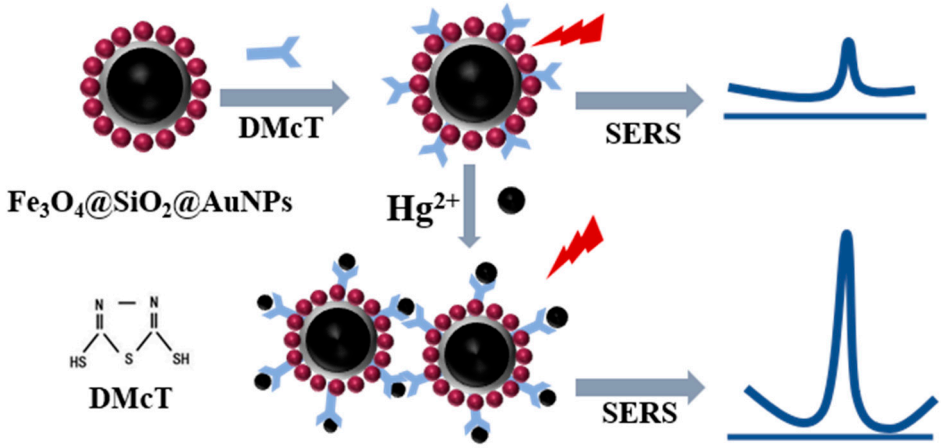

Figure 3. Schematic diagram of Hg^{2+} detection based on DMcT-functionalized Fe_3O_4@SiO_2@AuNPs.

3.4. SERS Detection of Hg^{2+}

As shown in Figure 4, there was no SERS signal for both Fe_3O_4@SiO_2 (Figure 4a) and Fe_3O_4@SiO_2@AuNPs (Figure 4b). The Raman spectral curve in Figure 4c shows the Raman signal of Fe_3O_4@SiO_2@AuNPs-DMcT in the absence of a magnetic field. The spectral curve in Figure 4d represents the SERS signals of Fe_3O_4@SiO_2@AuNPs-DMcT in the presence of the magnetic field. Compared with the spectral curve in Figure 4c, the Raman signal of DMcT was significantly enhanced in the magnetic field, which proved the enrichment effect of magnetic nanomaterials.

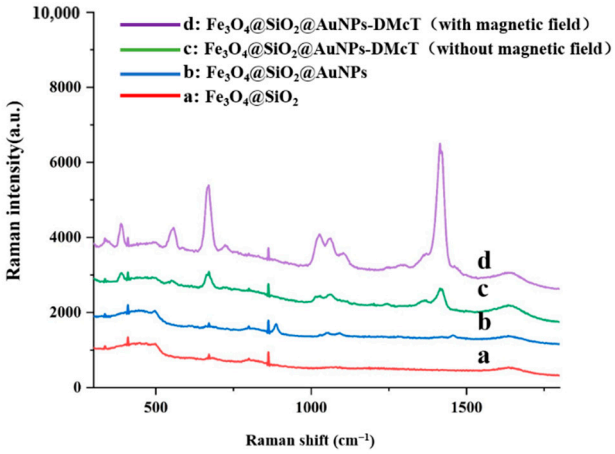

Figure 4. Raman spectra for different substrate states. (**a**): Fe_3O_4@SiO_2, (**b**): Fe_3O_4@SiO_2@AuNPs, (**c**): Fe_3O_4@SiO_2@AuNPs-DMcT without magnetic field, and (**d**): Fe_3O_4@SiO_2@AuNPs-DMcT with the magnetic field.

The SERS spectra of different concentrations of Hg^{2+} standard solution reacted with Fe_3O_4@SiO_2@AuNPs-DMcT for 10 min are shown in Figure 5A. The detection of Hg^{2+} was achieved by observing the increase in SERS intensity of DMcT. The Raman intensity at 1418 cm^{-1} represented the characteristic Raman peak of the C=N vibration in DMcT, which acted as a Hg^{2+} reporter and was enhanced with increasing Hg^{2+} concentration. The thiocarbonyl sulfur atom in DMcT was covalently bound to the Ag shell on the NP, and the N atom at the other end was used to recognize Hg^{2+}. The strong synergy between N-Hg guaranteed the functionalized NP aggregation of DMcT in the presence of Hg and enhanced the Raman signal. The Raman spectrum of DMcT showed vibrational peaks at 389, 554, 668, 1061, 1363, and 1418 cm^{-1}. The Raman peak assignments of DMcT are shown in Table 1. The intensity of the characteristic Raman peak of DMcT at 1418 cm^{-1} gradually increased with Hg^{2+} concentration, which was mainly due to the magnetic enrichment of Fe_3O_4. Fe_3O_4@SiO_2@AuNPs not only performed the substantial SERS enhancement

of AuNPs but also enriched the Hg^{2+} adsorbed on its surface. As shown in Figure 5B, the relative Raman intensity of DMcT showed an excellent linear relationship with the concentration of Hg^{2+} (0.5~80 ng/mL). The horizontal coordinate represents the Hg^{2+} concentration, and the vertical coordinate $R\text{-}R_0$ represents the difference in SERS intensity of DMcT at 1418 cm^{-1} when Hg^{2+} was present or absent. A good linear relationship was further obtained: y = 101.19x + 870.6, R^2 = 0.9709.

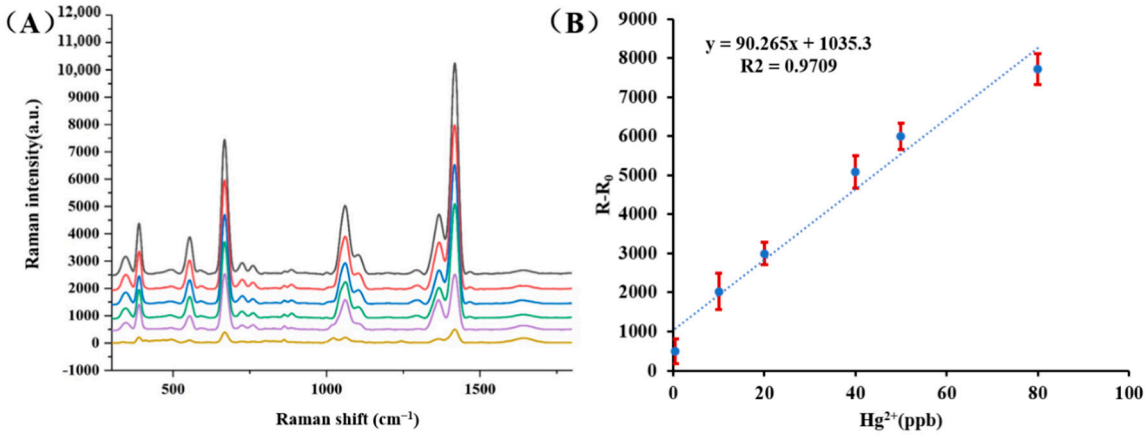

Figure 5. The Raman spectrum and standard curve for the detection of Hg^{2+} based on Fe_3O_4@SiO_2@AuNPs-DMcT SERS probes. (**A**) Raman spectra of the reaction between different concentrations of Hg^{2+} and Fe_3O_4@SiO_2@AuNPs-DMcT SERS probes; (**B**) linear relationship between Hg^{2+} concentration and SERS peak intensity at 1418 cm^{-1} for DMcT. ($R\text{-}R_0$, R, and R_0 represented the SERS intensity of DMcT at 1418 cm^{-1} when Hg^{2+} was present or absent).

Table 1. Spectral data and vibrational assignment of DMcT.

Raman DMcT Power	Raman Shift of DMcT	Assignment
1514 m	——	v (C=N) $_{asym}$
1456 vs	1418 vs 1363 m	v (C=N) $_{asym}$
1287 m	——	——
1120 w	——	Ring stretch
1089 m	1061 m	Ring stretch
1048 m	——	Ring stretch
725 m	668 s	v (C–S) $_{asym}$
666 s	554 m	o.p. dist.
545 m	——	
499 m	389 m	δ (CSC) + δ (CSH)
379 s	——	
322		o.p. dist.

s, strong; m, medium; w, weak; vs, very strong.

3.5. Enrichment of Hg^{2+} in Licorice Extract and SERS Detection

In order to verify the feasibility of magnetic nanomaterials for the detection of Hg^{2+}, we performed spiked recovery experiments for the content of Hg^{2+} in licorice extract. The spiked concentrations and detection results are shown in Table 2. Before the SERS assay, Hg^{2+} in the samples was adsorbed with an applied magnetic field, and the excess licorice extract was removed and resuspended in an equal volume of solution for testing. The results indicated that the spiked recoveries of Hg^{2+} in licorice extract by the magnetic nanomaterials combined with DMcT ranged from 89.10% to 111.00%, which met the methodological requirements and had practical application value.

Table 2. Detection of Hg^{2+} in licorice extract based on Fe_3O_4@SiO_2@AuNPs-DMcT.

Samples	Added	Detected	Recovery (%)	RSD (%) n = 5
Licorice extract	10 ng/mL	8.9 ng/mL	89.10	4.75
Licorice extract	30 ng/mL	33.3 ng/mL	111.00	5.39
Licorice extract	50 ng/mL	48.6 ng/mL	97.20	4.88
Licorice extract	80 ng/mL	77.1 ng/mL	96.37	6.97

3.6. Reproducibility and Specificity Examination

The reproducibility of the spectra was an essential factor in showing the practicality of the method. SERS was performed on Fe_3O_4@SiO_2@AuNPs-DMcT prepared from the same batch and the same concentration. The spectral reproducibility under eight parallel experiments is shown in Figure 6A. The RSD of DMcT at 1418 cm^{-1} was 7.46%, which indicated that the reproducibility of this method was strong. Next, Fe_3O_4@SiO_2@AuNPs stored in a refrigerator at 4 °C for 15 days were examined for stability, and it was found that their SERS signals were relatively stable. Fe_3O_4@SiO_2@AuNPs-DMcT had both high stability and the magnetic properties of AuNPs.

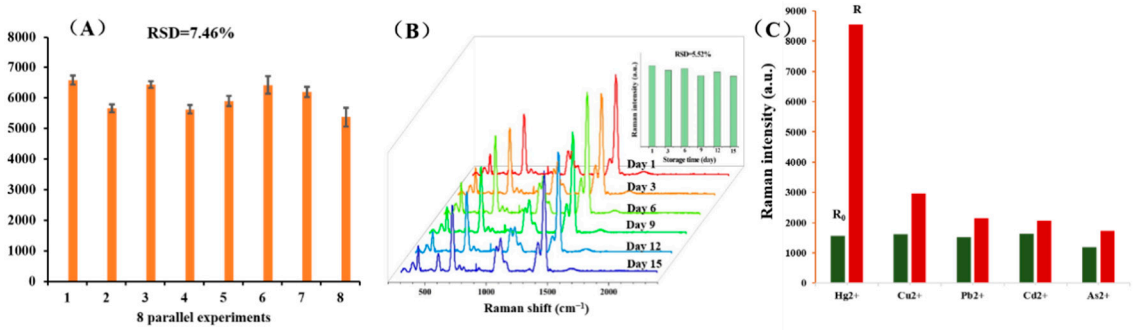

Figure 6. Reproducibility and stability experiments. (**A**) SERS spectra in eight parallel experiments; (**B**) SERS spectra of DMcT (10^{-5} mol/L) at different storage times for Fe_3O_4@SiO_2@AuNPs. (**C**) Selectivity of DMcT-functionalized Fe_3O_4@SiO_2@AuNPs for the detection of Hg^{2+}.

To verify the selectivity of Hg^{2+} detection based on DMcT-functionalized Fe_3O_4@SiO_2@AuNPs, four other more toxic heavy metal ions were selected as interfering ions for the detection. The concentrations of Pb^{2+}, Cd^{2+}, As^{3+} and Cu^{2+} were all 1000 ng/mL, except for Hg^{2+} which was 100 ng/mL. These concentrations were set to highlight the specificity of the material for adsorption of Hg^{2+}. The Raman detection results of these five heavy metal ions were analyzed, as shown in Figure 6C. The green bar graph represents the SERS signal before adding heavy metal ions, and the red bar graph represents the SERS signal after adding heavy metal ions. The change in the SERS signal indicated that the probe DMcT was highly selective to Hg^{2+}. This was most likely due to the fact that all N- atoms on DMcT form coordination structures with Hg^{2+}, and the known stability of coordination covalent bonds formed by nitrogen atoms. Hg^{2+} is higher than that of other heavy metal ions. Therefore, it showed superior specificity in Hg^{2+} detection.

3.7. Comparison with Other Substrate Materials

In order to highlight the superiority of the method in this paper, we compared the detection limits of Hg^{2+} based on SERS materials reported in the literature, as shown in Table 3. Compared with other SERS substrates, the magnetic nanomaterials used in this study have higher sensitivity, better separation, and stronger enrichment effects for the detection of Hg^{2+}.

Table 3. Comparison of different SERS substrate and Raman probes.

SERS Substrate	Raman Probes	Object	LOD (ng/mL)	Reference
AuNPs	Tryptophan	Hg^{2+}	5 ng/mL	[30]
Ag@AuNPs	TAMRA	Hg^{2+}	50 nmol/L	[31]
AgNPs	Dpy	Hg^{2+}	1 ng/mL	[32]
AuNPs	4-MBA	Hg^{2+}	50 ng/mL	[33]
Fe_3O_4@Ag	DMcT	Hg^{2+}	2 ng/mL	[34]
Fe_3O_4@SiO_2@AuNPs	DMcT	Hg^{2+}	0.5 ng/mL	This work

4. Conclusions

In this study, novel Fe_3O_4@SiO_2@AuNPs magnetic nanomaterials were prepared and combined with DMcT probe to enrich and detect heavy metals in TCM. The magnetic nanomaterials were synthesized through self-assembly, and their morphology and UV absorption were characterized. Using DMcT as the probe molecule, Hg^{2+} could bind to the nitrogen atoms in DMcT and induce the agglomeration of Fe_3O_4@SiO_2@AuNPs-DMcT, leading to the enhancement of SERS signal. Through the methodological investigation, the detection of Hg^{2+} in the licorice extracts by SERS proved that the material had the advantages of high sensitivity, low detection limit, and effective separation and enrichment. The method showed good linearity between 0.5 and 80 ng/mL (R^2 = 0.9709). It also achieved high recoveries (89.10~111.00%) in the detection of licorice extracts, indicating potential value in applying SERS to detect heavy metal ions in complex matrices. The method has shown strong application prospects in the rapid on-site trace detection of heavy metal ions in traditional Chinese medicine.

Author Contributions: J.Z.: formal analysis, conceptualization, and methodology. B.W.: investigation, data curation, and writing—original draft preparation. J.L. and P.Y.: supervision and validation. G.X. and J.Y. (Jiangyu Yao): data curation. X.G.: software and formal analysis, J.Y. (Jizhong Yan): project administration and supervision. H.Z.: funding acquisition, reviewing, and editing All authors have read and agreed to the published version of the manuscript.

Funding: This research was supported by Zhejiang Provincial Natural Science Foundation of China (Grant No. LY20H280014), the Basic Public Welfare Research Project of Zhejiang Province (Grant No. LBY22H280003), and Zhejiang Provincial Department of Science and Technology Project (Grant No. 2022C03062).

Institutional Review Board Statement: Not applicable.

Informed Consent Statement: Not applicable.

Data Availability Statement: Not applicable.

Conflicts of Interest: The authors declare that they have no known competing financial interests or personal relationships that could have appeared to influence the work reported in this paper.

References

1. Li, L.; Wu, Y.; Wang, J.; Yan, H.; Lu, J.; Wang, Y.; Zhang, B.; Zhang, J.; Yang, J.; Wang, X.; et al. Potential treatment of COVID-19 with traditional chinese medicine: What herbs can help win the battle with SARS-CoV-2? *Engineering* **2021**, *in press*. [CrossRef]
2. Zhu, Y.Z.; He, Z.P.; Zhang, M. Effects of traditional Chinese medicine in the prevention and treatment of pulmonary fibrosis in recovery from novel coronavirus pneumonia (COVID-19). *Chin. Tradit. Pat. Med.* **2021**, *43*, 2224–2229.
3. Meng, C.; Wang, P.; Hao, Z. Ecological and health risk assessment of heavy metals in soil and Chinese herbal medicines. *Environ. Geochem. Health* **2021**, *44*, 817–828. [CrossRef] [PubMed]
4. Liang, X.; Yan, L.; Xu, X. Study on the excessive heavy metal in teaditional Chinese medicine. *Guangxi J. Tradit. Chin. Med.* **2021**, *44*, 75–77.
5. Li, M.T.; Li, P.C.; Lin, D.J. Detection Research progress of Hg (II) by Surface-enhanced Raman Spectroscopy. *Technol. Dev. Chem. Ind.* **2020**, *49*, 43–45+72.
6. Jiang, Z.G.; Xu, N.; Liu, B.X. Metal concentrations and risk assessment in water, sediment and economic fish species with various habitat preferences and trophic guilds from Lake Caizi, Southeast China. *Ecotoxicol. Environ. Saf.* **2018**, *157*, 1–8. [CrossRef]

7. Wu, D.H. Determination of Mercury Content in Rhizome Traditional Chinese Medicine Pieces by Mercury Analyzer. *J. Insp. Quar.* **2019**, *29*, 38–39.
8. Hassan, S.; Mazhar, W.; Farooq, S.; Ali, A.; Musharraf, S.G. Assessment of heavy metals in calcium carbide treated mangoes by inductively coupled plasmamass spectrometry (ICP-MS). *Food Addit. Contam. Part A* **2019**, *36*, 1769–1776. [CrossRef] [PubMed]
9. Li, K.; Yang, H.; Yuan, X.; Zhang, M. Recent developments of heavy metals detection in traditional Chinese medicine by atomic spectrometry. *Microchem. J.* **2021**, *160*, 105726. [CrossRef]
10. Ding, Q.; Li, C.; Wang, H.; Xu, C.; Kuang, H. Electrochemical detection of heavy metal ions in water. *Chem. Commun.* **2021**, *57*, 7215–7231. [CrossRef] [PubMed]
11. Wang, Q.; Wei, K.N.; Huang, S.Z.; Tang, Q.; Tao, Z.; Huang, Y. "Turn-Off" Supramolecular Fluorescence Array Sensor for Heavy Metal Ion Identification. *ACS Omega* **2021**, *6*, 31229–31235. [CrossRef] [PubMed]
12. Kamar, V.; Dağalp, R.; Taştekin, M. Determination of Heavy Metals in Almonds and Mistletoe as a Parasite Growing on the Almond Tree Using ICP-OES or ICP-MS. *Biol. Trace Elem. Res.* **2018**, *185*, 226–235. [CrossRef] [PubMed]
13. Yu, L.; Pang, Y.; Mo, Z.; Huang, Y.; Shen, X. Coordination array for accurate colorimetric sensing of multiple heavy metal ions. *Talanta* **2021**, *231*, 122357–122364. [CrossRef]
14. Fan, M.; Andrade, G.F.; Brolo, A.G. A review on the fabrication of substrates for surface enhanced Raman spectroscopy and their applications in analytical chemistry. *Anal. Chim. Acta* **2011**, *693*, 7–25. [CrossRef] [PubMed]
15. Jiang, Y.; Sun, D.W.; Pu, H.; Wei, Q. Surface enhanced Raman spectroscopy (SERS): A novel reliable technique for rapid detection of common harmful chemical residues. *Trends Food Sci. Technol.* **2018**, *75*, 10–22. [CrossRef]
16. Jamieson, L.E.; Asiala, S.M.; Gracie, K.; Faulds, K.; Graham, D. Bioanalytical Measurements Enabled by Surface-Enhanced Raman Scattering (SERS) Probes. *Annu. Rev. Anal. Chem.* **2017**, *10*, 415–437. [CrossRef] [PubMed]
17. Zhang, D.; Liang, P.; Chen, W.; Tang, Z.; Li, C.; Xiao, K.; Jin, S.; Ni, D.; Yu, Z. Rapid field trace detection of pesticide residue in food based on surface-enhanced Raman spectroscopy. *Microchim. Acta* **2021**, *188*, 370–389. [CrossRef] [PubMed]
18. Wang, T.; Wang, S.P.; Cheng, Z.H. Emerging core–shell nanostructures for surface-enhanced Raman scattering (SERS) detection of pesticide residues. *Chem. Eng. J.* **2021**, *424*, 130323–130328. [CrossRef]
19. Wang, T.; Wei, J.C.; Wang, Y.T.; Li, P. Recent advances in surface-enhanced Raman scattering technique for pollutant detection in Chinese medicinal material. *China J. Chin. Mater. Med.* **2021**, *46*, 62–71.
20. Zuo, F.T.; Xu, W.; Zhao, A.W. A SERS Approach for Rapid Detection of Hg^{2+} Based on Functionalized Fe_3O_4@Ag Nanoparticles. *Acta Chim. Sin.* **2019**, *77*, 379–386. [CrossRef]
21. Song, C.Y.; Yang, B.Y.; Yang, Y.J. SERS-based mercury ion detections: Principles, strategies and recent advances. *Sci. China Chem.* **2016**, *59*, 16–29. [CrossRef]
22. Wang, C.W.; Rong, Z.; Wang, J. Seed-mediated synthesis of high-performance silver-coated magnetic nanoparticles and their use as effective SERS substrates. *Colloids Surf. A Physicochem. Eng. Asp.* **2016**, *506*, 393–401. [CrossRef]
23. Xu, Y.J.; Haung, S.; Li, L.J.; Cheng, H.; Huang, W.Y.; Feng, J. Preparation of Fe_3O_4@SiO_2@Ag Nanocomposites and Detection of Oxacillin by Surface-enhanced Raman Spectroscopy. *J. Anal. Sci.* **2020**, *36*, 7–12.
24. Wang, H.; Shen, J.; Cao, G.X. Multifunctional PEG encapsulated Fe_3O_4@silver hybrid nanoparticles: Antibacterial activity, cell imaging and combined photothermo/chemo-therapy. *J. Mater. Chem. B* **2013**, *1*, 6225–6234. [CrossRef]
25. Shen, J.H.; Zhu, Y.H.; Yang, X.L. Multifunctional Fe_3O_4@Ag/SiO_2/Au Core-Shell Microspheres as a Novel SERS-Activity Label via Long-Range Plasmon Coupling. *Langmuir* **2013**, *29*, 690–695. [CrossRef] [PubMed]
26. Sun, Z.L.; Du, J.J.; Yan, L. Multifunctional Fe_3O_4@SiO_2-Au Satellite Structured SERS Probe for Charge Selective Detection of Food Dyes. *ACS Appl. Mater. Interfaces* **2016**, *8*, 3056–3062. [CrossRef] [PubMed]
27. Maximenko, A.; Depciuch, J.; Łopuszyńska, N.; Stec, M. Fe_3O_4@SiO_2@Au nanoparticles for MRI-guided chemo/NIR photothermal therapy of cancer cells. *RSC Adv.* **2020**, *10*, 26508–26520. [CrossRef] [PubMed]
28. Stöber, W.; Fink, A.; Bohn, E. Controlled growth of monodisperse silica spheres in the micron size range. *J. Colloid Interface Sci.* **1968**, *26*, 62–69. [CrossRef]
29. Chen, J.L.; Yang, P.C.; Wu, T. Determination of mercury (II) ions based on silver-nanoparticles-assisted growth of gold nanostructures: UV–Vis and surface enhanced Raman scattering approaches. *Spectrochim. Acta Part A Mol. Biomol. Spectrosc.* **2018**, *199*, 301–307. [CrossRef]
30. Senapati, T.; Senapati, D.; Singh, A.K. Highly selective SERS probe for Hg(ii) detection using tryptophan-protected popcorn shaped gold nanoparticles. *Chem. Commun.* **2011**, *47*, 10326. [CrossRef]
31. Han, D.; Lim, S.Y.; Kim, B.J. Mercury(ii) detection by SERS based on a single gold microshell. *Chem. Commun.* **2010**, *46*, 5587. [CrossRef] [PubMed]
32. Zhao, Y.; Yamaguchi, Y.; Ni, Y.; Li, M.; Dou, X. A SERS-based capillary sensor for the detection ofmercury ions in environmental water. *Spectrochim. Acta Part A Mol. Biomol. Spectrosc.* **2020**, *233*, 118193. [CrossRef]
33. Tan, X.; Liu, X.B.; Bai, H.J. Quantitative detection of several heavy metals by modified surface-enhanced Raman substrates. *J. Sichuan Univ. (Nat. Sci. Ed.)* **2021**, *58*, 148–154.
34. Chen, Z.Y.; Gupta, A.; Chattopadhyay, S. Detection of mercury in spiked cosmetics by surface enhanced Raman spectroscopy using silver shelled iron oxide nanoparticles. *Sens. Actuators B Chem.* **2021**, *337*, 129788. [CrossRef]